Journal of the Korean Physical Society, Vol. 57, No. 1, July 2010, pp. 23∼29

Strange Nonchaotic Spiking in the Quasiperiodically-forced Hodgkin-Huxley Neuron

Woochang LIM* and Sang-Yoon KIM†
Department of Physics, Kangwon National University, Chuncheon 200-701

(Received 3 June 2010)

We study the transition from a silent state to a spiking state by varying the dc stimulus in the quasiperiodically-forced Hodgkin-Huxley neuron. For this quasiperiodically-forced case, a new type of strange nonchaotic (SN) spiking state is found to appear between the silent state and the chaotic spiking state as intermediate one. Using a rational approximation to the quasiperiodic forcing, we investigate the mechanism for the appearance of such an SN spiking state. We thus find that a smooth torus (corresponding to the silent state) is transformed into an SN spiking attractor via a phase-dependent saddle-node bifurcation. This is in contrast to the periodically-forced case where the silent state transforms directly to a chaotic spiking state. SN spiking states are characterized in terms of the interspike interval, so they are found to be aperiodic complex ones, as in the case of chaotic spiking states. Hence, aperiodic complex spikings may result from two dynamically different states with strange geometry (one is chaotic and the other one is nonchaotic).

PACS numbers: 05.45.Ac, 05.45.Df, 87.19.L-
Keywords: Strange nonchaotic spiking, Quasiperiodically-forced neuron
DOI: 10.3938/jkps.57.23

I. INTRODUCTION

To probe the dynamical properties of a system, one often applies an external stimulus to the system and investigate its response. Particularly, periodically stimulated biological oscillators have attracted much attention in various systems such as the embryonic chick heart-cell aggregates [1], squid giant axons [2,3], and cortical pyramidal neurons [4]. These periodically-stimulated systems have been found to exhibit rich regular (such as phase locking and quasiperiodicity) and chaotic responses [5, 6]. On the other hand, the quasiperiodically forced case has received little attention [7,8]. Hence, it is necessary to make further intensive investigations on the dynamical responses of quasiperiodically-forced biological oscillators.

Strange nonchaotic (SN) attractors typically appear in quasiperiodically-forced dynamical systems [9–12]. They exhibit some properties of regular as well as chaotic attractors. Like regular attractors, their dynamics is nonchaotic in the sense that they do not have a positive Lyapunov exponent; like usual chaotic attractors, they have a geometrically strange (fractal) structure. Here, we are interested in the dynamical behaviors of quasiperiodically-forced neurons, and SN spikings are expected to occur.

*E-mail: wclim@kangwon.ac.kr
†Corresponding Author; E-mail: sykim@kangwon.ac.kr

This paper is organized as follows. In Sec. II., we consider the Hodgkin-Huxley (HH) model neuron, which was originally introduced to describe the behavior of the squid giant axon [13], and investigate the transition from a silent state to a spiking state by varying the dc stimulus. This work is in contrast to previous works on the effect of periodic and quasiperiodic forcings on the HH neuron in the spiking state of self-sustained oscillations of the membrane potential [3,8,14]. For the periodically-forced case (*i.e.*, in the presence of only one ac stimulus source), an intermittent transition from a silent state (with subthreshold oscillation) to a chaotic spiking state occurs when the dc stimulus passes a threshold value. The effect of the quasiperiodic forcing on this intermittent route to chaotic spiking is investigated by adding another independent ac stimulus source. Thus, a new type of SN spiking is found to occur between the silent state and the chaotic spiking state. Using a rational approximation to the quasiperiodic forcing [11, 12], we investigate the mechanism for the appearance of such SN spikings. Thus, a smooth torus, corresponding to a silent state, is found to transform to an SN spiking attractor via a phase-dependent saddle-node bifurcation. Together with chaotic spikings, these SN spikings are characterized in terms of the interspike interval. Both the chaotic and the SN spiking states are found to be aperiodic complex ones. Such aperiodic complexity comes from the strange geometry of both spiking states with qualitatively different dynamics (one is chaotic and the

other is nonchaotic). These complex spikings might be one of the origins of the complex physiological rhythms which are central to life [6]. Finally, a summary is given in Sec. III.

II. SN SPIKINGS IN THE QUASIPERIODICALLY-FORCED HH NEURON

We consider the conductance-based HH neuron model, which serves as a canonical model for spiking neurons [13]. The dynamics of the HH neuron, which is quasiperiodically forced at two incommensurate frequencies f_1 and f_2, is governed by the following set of differential equations:

$$\begin{aligned} C\frac{dV}{dt} &= -I_{ion} + I_{ext} = -(I_{Na} + I_K + I_L) + I_{ext} \\ &= -g_{Na} m^3 h (V - V_{Na}) - g_K n^4 (V - V_K) \\ &\quad -g_L (V - V_L) + I_{ext}, \qquad (1a) \\ \frac{dx}{dt} &= \alpha_x(V)(1-x) - \beta_x(V) x; \quad x = m, h, n, \qquad (1b) \end{aligned}$$

where the external stimulus current density (measured in units of μA/cm^2) is given by $I_{ext} = I_{dc} + A_1 \sin(2\pi f_1 t) + A_2 \sin(2\pi f_2 t)$, I_{dc} is a dc stimulus, A_1 and A_2 are amplitudes of quasiperiodic forcing, and $\omega (\equiv f_2/f_1)$ is irrational (f_1 and f_2: measured in units of kHz). Here, the state of the HH neuron at a time t [measured in units of millisecond (ms)] is characterized by four variables: the membrane potential V (measured in units of mV), the activation (inactivation) gate variable $m\,(h)$ of the Na^+ channel [*i.e.,* the fraction of sodium channels with open activation (inactivation) gates], and the activation gate variable n of the K^+ channel (*i.e.,* the fraction of potassium channels with open activation gates). In Eq. (1a), C represents the membrane capacitance per surface unit (measured in units of μF/cm^2) and the total ionic current I_{ion} consists of the sodium current I_{Na}, the potassium current I_K, and the leakage current I_L. Each ionic current obeys Ohm's law. The constants g_{Na}, g_K, and g_L are the maximum conductances for the ion and the leakage channels, and the constants V_{Na}, V_K, and V_L are the reversal potentials at which each current is balanced by the ionic concentration difference across the membrane. The three gate variables obey the first-order kinetics of Eq. (1b). The rate constants are given by

$$\begin{aligned} \alpha_m(V) &= \frac{0.1[25 - (V - V_r)]}{\exp[\{25 - (V - V_r)\}/10] - 1}, \\ \beta_m(V) &= 4 \exp[-(V - V_r)/18], \qquad (2a) \\ \alpha_h(V) &= 0.07 \exp[-(V - V_r)/20], \\ \beta_h(V) &= \frac{1}{\exp[\{30 - (V - V_r)\}/10] + 1}, \qquad (2b) \\ \alpha_n(V) &= \frac{0.01[10 - (V - V_r)]}{\exp[\{10 - (V - V_r)\}/10] - 1}, \\ \beta_n(V) &= 0.125 \exp[-(V - V_r)/80], \qquad (2c) \end{aligned}$$

where V_r is the resting potential when $I_{ext} = 0$. For the squid giant axon, typical values of the parameters (at 6.3 °C) are: $C = 1\mu$F/cm^2, $g_{Na} = 120$ mS/cm^2, $g_K = 36$ mS/cm^2, $g_L = 0.3$ mS/cm^2, $V_{Na} = 50$ mV, $V_K = -77$ mV, $V_L = -54.4$ mV, and $V_r = -65$ mV [15].

To obtain the Poincaré map of Eq. (1), we make a normalization $f_1 t \to t$; then, Eq. (1) can be reduced to the following differential equations:

$$\begin{aligned} \frac{dV}{dt} &= F_1(\mathbf{x}, \theta) \\ &= \frac{1}{C\ f_1}[-g_{Na} m^3 h (V - V_{Na}) - g_K n^4 (V - V_K) \\ &\quad - g_L (V - V_L) + I_{ext}], \qquad (3a) \\ \frac{dm}{dt} &= F_2(\mathbf{x}, \theta) = \frac{1}{f_1}[\alpha_m(V)(1-m) - \beta_m(V) m], \\ &\qquad (3b) \\ \frac{dh}{dt} &= F_3(\mathbf{x}, \theta) = \frac{1}{f_1}[\alpha_h(V)(1-h) - \beta_h(V) h], \quad (3c) \\ \frac{dn}{dt} &= F_4(\mathbf{x}, \theta) = \frac{1}{f_1}[\alpha_n(V)(1-n) - \beta_n(V) n], \quad (3d) \\ \frac{d\theta}{dt} &= \omega \pmod 1, \qquad (3e) \end{aligned}$$

where $\mathbf{x}[= (x_1, x_2, x_3, x_4)] \equiv (V, m, h, n)$ and $I_{ext} = I_{dc} + A_1 \sin(2\pi t) + A_2 \sin(2\pi\theta)$. The phase space of the quasiperiodically-forced HH oscillator is six dimensional with coordinates V, m, h, n, θ, and t. Because the system is periodic in θ and t, they are circular coordinates in the phase space. Then, we consider the surface of a section, the V-m-h-n-θ hypersurface at $t = n$ (n: integer). The phase-space trajectory intersects with the surface of a section at a sequence of points. This sequence of points corresponds to a mapping on the five-dimensional hypersurface. The map can be computed by stroboscopically sampling the orbit points $\mathbf{v}_n$ [$\equiv (\mathbf{x}_n, \theta_n)$] at the discrete time n (corresponding to multiples of the first external driving period T_1). We call the transformation $\mathbf{v}_n \to \mathbf{v}_{n+1}$ the Poincaré map and write $\mathbf{v}_{n+1} = P(\mathbf{v}_n)$.

Numerical integrations of Eqs. (1) and (3) are done using the fourth-order Runge-Kutta method. A dynamical analysis is performed in both the continuous-time system (*i.e.*, flow) and the discrete-time system (*i.e.*, Poincaré map). For example, the time series of the membrane potential $V(t)$, the phase flow, and the interspike interval are obtained in the flow. On the other hand, the Lyapunov exponent [16] and the phase sensitivity exponent [11] of an attractor are calculated in the Poincaré map. To obtain the Lyapunov exponent of an attractor in the Poincaré map, we choose 20 random initial points $\{(V_i(0), m_i(0), h_i(0), n_i(0), \theta_i(0)); i = 1, \ldots, 20\}$ with uniform probability in the range of $V_i(0) \in (-60, 20)$, $m_i(0) \in (0.2, 0.8)$, $h_i(0) \in (0.1, 0.5)$, $n_i(0) \in (0.4, 0.7)$, and $\theta_i(0) \in [0, 1)$. For each initial

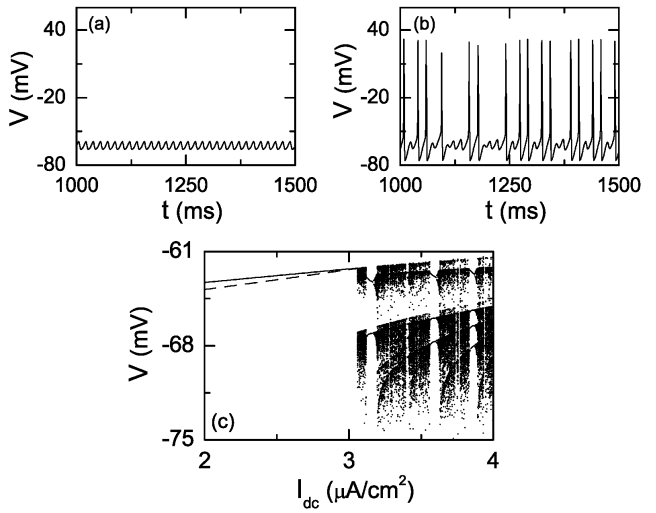

Fig. 1. Intermittent transition to a chaotic spiking state for the case of periodic forcing with $A_1 = 1.0\ \mu\text{A/cm}^2$ and $f_1 = 60$ Hz ($A_2 = 0$). (a) Time series of $V(t)$ for the silent state exhibiting subthreshold oscillations for $I_{\rm dc} = 2.5\ \mu\text{A/cm}^2$. (b) Time series of $V(t)$ for the chaotic spiking state with $\sigma_1 \simeq 0.247$ for $I_{\rm dc} = 3.5\ \mu\text{A/cm}^2$. (c) Bifurcation diagram (*i.e.*, plot of V versus $I_{\rm dc}$) in the Poincaré map. We obtain attractors by iterating the Poincaré map at 500 equally-spaced values of $I_{\rm dc}$ in the range of $I_{\rm dc} \in [2, 4]$. For each chosen $I_{\rm dc}$, we choose a random initial point $(V(0), m(0), h(0), n(0), \theta(0))$ with uniform probability in the range of $V(0) \in (-60, 20)$, $m(0) \in (0.2, 0.8)$, $h(0) \in (0.1, 0.5)$, $n(0) \in (0.4, 0.7)$, and $\theta(0) \in [0, 1)$, and obtain the attractor through 200-times iterations of the Poincaré map after transients of the 1000 Poincaré maps.

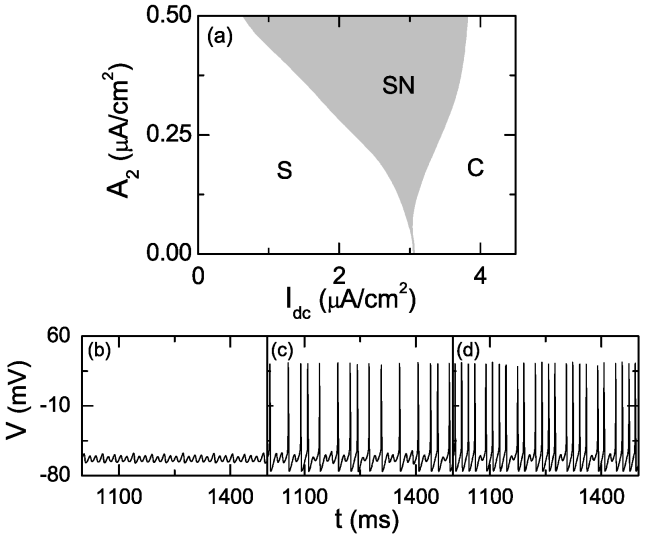

Fig. 2. Appearance of SN spiking states for the quasiperiodically-forced case when $A_1 = 1.0\ \mu\text{A/cm}^2$ and $f_1 = 60$ Hz. (a) State diagram in the $I_{dc} - A_2$ plane. Silent, SN, and chaotic states are represented by **S**, **SN**, and **C**, respectively. We set $A_2 = 0.3\ \mu\text{A/cm}^2$. Time series of $V(t)$ of (b) the silent state for $I_{dc} = 1.7\ \mu\text{A/cm}^2$, (c) the SN spiking state for $I_{dc} = 2.85\ \mu\text{A/cm}^2$, and (d) the chaotic spiking state for $I_{dc} = 3.9\ \mu\text{A/cm}^2$.

point, we get the Lyapunov exponent [16] and choose the average value of the 20 Lyapunov exponents. (The method of obtaining the phase sensitivity exponent will be explained below.)

Here, we set ω to be the reciprocal of the golden mean [*i.e.*, $\omega = (\sqrt{5} - 1)/2$] and numerically investigate dynamical transition from a silent state to a spiking state by varying I_{dc} in the HH neuron under external stimulus. We first consider the case of periodic forcing (*i.e.*, $A_2 = 0$) when $A_1 = 1.0\ \mu\text{A/cm}^2$ and $f_1 = 60$ Hz. Figure 1(a) shows the time series of $V(t)$ for the silent state when $I_{dc} = 2.5\ \mu\text{A/cm}^2$. We note that this silent state with the largest Lyapunov exponent $\sigma_1 \simeq -1.569$ exhibits subthreshold oscillations. As I_{dc} passes a threshold value of $I_{dc} = 3.058\,824\ \mu\text{A/cm}^2$, a chaotic spiking state appears, as shown in Fig. 1(b) for $I_{dc} = 3.5\ \mu\text{A/cm}^2$. This transition from a silent state to a chaotic spiking state is investigated by varying I_{dc} in the Poincaré map. Figure 1(c) shows the bifurcation diagram (*i.e.*, plot of V versus I_{dc}). The solid curve represents a stable fixed point corresponding to the silent state. The stable fixed point loses its stability for $I_{dc} = 3.058\,824\ \mu\text{A/cm}^2$ via a saddle-node bifurcation when it absorbs the unstable fixed point denoted by the dashed curve, and then a chaotic spiking attractor, corresponding to a chaotic spiking state, appears.

From now on, we consider the quasiperiodically forced case when $A_1 = 1.0\,\mu\text{A/cm}^2$ and $f_1 = 60\,\text{Hz}$. Figure 2(a) shows a state diagram in the $I_{dc} - A_2$ plane. Each state is characterized by both the largest (nontrivial) Lyapunov exponent σ_1, associated with dynamics of the variable **x** [besides the (trivial) zero exponent, related to the phase variable θ of the quasiperiodic forcing] and the phase sensitivity exponent δ. The exponent δ measures the sensitivity of the variable **x** with respect to the phase θ of the quasiperiodic forcing and characterizes the strangeness of an attractor [11]. A (regular) silent state, which has a negative Lyapunov exponent (*i.e.*, $\sigma_1 < 0$) and has no phase sensitivity (*i.e.* $\delta = 0$), exists in the region represented by **S**. On the other hand, a chaotic spiking state, which has a positive Lyapunov exponent $\sigma_1 > 0$, exists in the region denoted by **C**. Between these regular and chaotic regions, a new type of SN spiking state that has a negative Lyapunov exponent ($\sigma_1 < 0$) and a positive phase sensitivity exponent ($\delta > 0$) exist in the region represented by **SN**. Due to their high phase sensitivity, SN spiking states have a strange fractal phase-space structure. As an example, we consider the case of $A_2 = 0.3$ $\mu\text{A/cm}^2$ and investigate the dynamical behaviors of the quasiperiodically forced HH neuron by varying $I_{\rm dc}$. As I_{dc} passes a threshold I^*_{dc} ($\simeq$1.9169 $\mu\text{A/cm}^2$), the silent state becomes unstable, and a transition to an SN spiking state occurs. As I_{dc} is further increased and passes another threshold value of $I_{dc} \simeq 3.572\ \mu\text{A/cm}^2$, the SN

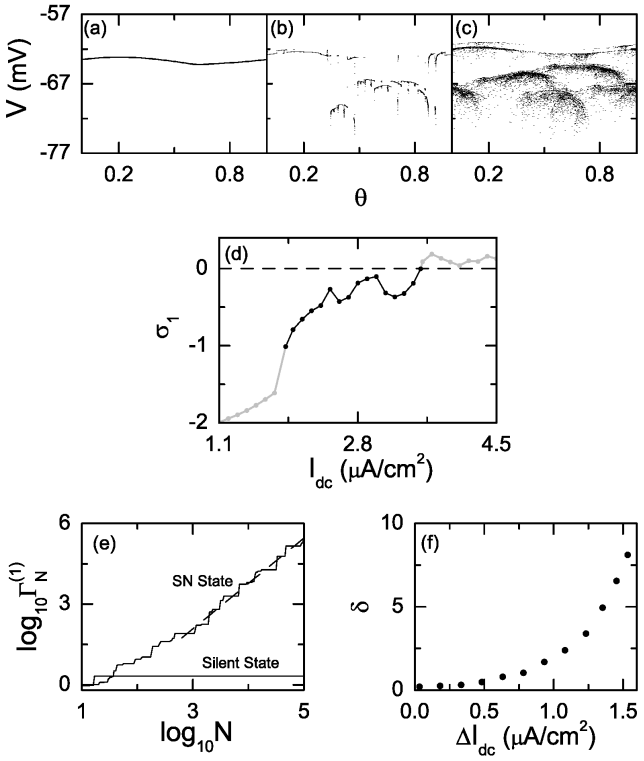

Fig. 3. Characterization of the silent and the spiking states for $A_1 = 1.0$ μA/cm^2, $A_2 = 0.3$ μA/cm^2, and $f_1 = 60$ Hz. Projections of attractors onto the $\theta - V$ plane in the Poincaré map are shown for the (a) silent, (b) SN spiking, and (c) chaotic spiking states when $I_{dc} = 1.7$, 2.85, and 3.9 μA/cm^2, respectively. (d) Lyapunov-exponent (σ_1) diagram (*i.e.,* plot of σ_1 versus $I_{\rm dc}$); for the SN spiking attractor is shown in black. (e) Phase-sensitivity functions $\Gamma_N^{(1)}$ are shown for the silent and the SN spiking attractors when $I_{dc} = 1.7$ and 2.85 μA/cm^2, respectively. For the SN spiking attractor, the graph is well fitted with a dashed straight line with slope $\delta \simeq 1.69$. (f) Plot of the phase-sensitivity exponent δ versus $\Delta I_{\rm dc}$ ($= I_{\rm dc} - I_{\rm dc}^*$) for the SN spiking attractor; $I_{\rm dc}^* \simeq 1.9169$ μA/cm^2.

spiking state transforms to a chaotic spiking state. Figures 2(b) - 2(d) show the time series of the membrane potential $V(t)$ of a silent state (exhibiting subthreshold oscillations), an SN spiking state, and a chaotic spiking state for $I_{\rm dc} = 1.7$, 2.85, and 3.9 μA/cm^2, respectively.

The silent and the spiking states for $A_2 = 0.3$ μA/cm^2 are analyzed in terms of the largest Lyapunov exponent σ_1 and the phase sensitivity exponent δ in the Poincaré map. Projections of attractors onto the $\theta - V$ plane for the above three cases are given in Figs. 3(a) - 3(c), respectively. For the silent case, a smooth torus exists in the $\theta - V$ plane [see Fig. 3(a)]. On the other hand, nonsmooth spiking attractors appear for both SN and chaotic spiking states, as shown in Figs. 3(b) and 3(c). A dynamical property of each state is characterized in terms of the largest Lyapunov exponent σ_1 (measuring the degree of sensitivity to initial conditions). The Lyapunov-exponent diagram is given in Fig. 3(d). When passing the spiking transition point $I_{dc}^*(\simeq 1.9169$ μA/cm$^2)$, an SN spiking attractor appears. The graph of σ_1 for the SN spiking state is shown in black, and its value is negative as in the case of a smooth torus. However, as I_{dc} passes the chaotic transition point I_{dc} ($\simeq 3.572$ μA/cm^2), a chaotic spiking attractor with a positive σ_1 appears. Although SN and chaotic spiking attractors are dynamically different, they both have strange geometry, leading to aperiodic complex spikings. To characterize the strangeness of an attractor, we investigate the sensitivity of the attractor with respect to the phase θ of the external quasiperiodic forcing [11]. This phase sensitivity may be characterized by differentiating $\mathbf{x}$ with respect to θ at a discrete time $t = n$. Using Eq. (3), we may obtain the following governing equation for $\frac{\partial x_i}{\partial \theta}$ $(i = 1, 2, 3, 4)$:

$$\frac{d}{dt}\left(\frac{\partial x_i}{\partial \theta}\right) = \sum_{j=1}^{4} \frac{\partial F_i}{\partial x_j} \cdot \frac{\partial x_j}{\partial \theta} + \frac{\partial F_i}{\partial \theta}, \tag{4}$$

where $(x_1, x_2, x_3, x_4) = (V, m, h, n)$ and F_i's $(i = 1, 2, 3, 4)$ are given in Eq. (3). Starting from an initial point $(\mathbf{x}(0), \theta(0))$ and an initial value $\partial \mathbf{x}/\partial\theta = \mathbf{0}$ for $t = 0$, we may obtain the derivative values of $S_n^{(i)}$ $(\equiv \partial x_i/\partial\theta)$ at all subsequent discrete time $t = n$ by integrating Eqs. (3) and (4). One can easily see the boundedness of $S_n^{(i)}$ by looking only at the maximum

$$\gamma_N^{(i)}(\mathbf{x}(0), \theta(0)) = \max_{0 \le n \le N} |S_n^{(i)}(\mathbf{x}(0), \theta(0))| \ \ (i = 1, 2, 3, 4). \tag{5}$$

We note that $\gamma_N^{(i)}(\mathbf{x}(0), \theta(0))$ depends on a particular trajectory. To obtain a "representative" quantity that is independent of a particular trajectory, we consider an ensemble of randomly chosen initial points $\{(\mathbf{x}(0), \theta(0))\}$ and take the minimum value of $\gamma_N^{(i)}$ with respect to the initial orbit points [11],

$$\Gamma_N^{(i)} = \min_{\{(\mathbf{x}(0), \theta(0))\}} \gamma_N^{(i)}(\mathbf{x}(0), \theta(0)) \ \ (i = 1, 2, 3, 4). \tag{6}$$

Figure 3(e) shows a phase sensitivity function $\Gamma_N^{(1)}$, which is obtained in an ensemble containing 20 random initial orbit points $\{(V_i(0), m_i(0), h_i(0), n_i(0), \theta_i(0)); i = 1, \ldots, 20\}$ that are chosen with uniform probability in the range of $V_i(0) \in (-60, 20)$, $m_i(0) \in (0.2, 0.8)$, $h_i(0) \in (0.1, 0.5)$, $n_i(0) \in (0.4, 0.7)$ and $\theta_i(0) \in [0, 1)$. For the silent case of $I_{dc} = 1.7$, $\Gamma_N^{(1)}$ grows up to the largest possible value of the derivative $|\partial x_1/\partial\theta|$ along a trajectory and remains there for all subsequent time. Thus, $\Gamma_N^{(1)}$ saturates for large N; hence, the silent state has no phase sensitivity (*i.e.*, it has smooth geometry). On the other hand, for the case of SN spiking, $\Gamma_N^{(i)}$ grows unboundedly with the same power δ, independently of i:

$$\Gamma_N^{(i)} \sim N^{\delta}. \tag{7}$$

Here, the value of $\delta \simeq 1.69$ is a quantitative characteristic of the phase sensitivity of the SN spiking attractor for $I_{dc} = 2.85$ μA/cm^2, and δ is called the phase sensitivity exponent. For obtaining satisfactory statistics, we consider 20 ensembles for each I_{dc}, each of which contains 20 randomly-chosen initial points and choose the average value of the 20 phase sensitivity exponents obtained in the 20 ensembles. Figure 3(f) shows a plot of δ versus $\Delta I_{\rm dc}$ $(= I_{\rm dc} - I^*_{\rm dc})$. Note that the value of δ monotonically increases from zero as I_{dc} is increased away from the spiking transition point I^*_{dc} ($\simeq$1.9169 μA/cm^2). As a result of this phase sensitivity, the SN spiking attractor has strange geometry, leading to aperiodic complex spikings, as in the case of the chaotic spiking attractor.

Using the rational approximation to the quasiperiodic forcing, we explain the mechanism for the transition from a silent to an SN spiking state. For the inverse golden mean, its rational approximants are given by the ratios of the Fibonacci numbers, $\omega_k = F_{k-1}/F_k$, where the sequence of $\{F_k\}$ satisfies $F_{k+1} = F_k + F_{k-1}$ with $F_0 = 0$ and $F_1 = 1$. Instead of the quasiperiodically forced system, we study an infinite sequence of periodically forced systems with rational driving frequencies ω_k. For each rational approximation of level k, a periodically-forced system has a periodic or a chaotic attractor that depends on the initial phase θ_0 of the external forcing. Then, the union of all attractors for different θ_0 gives the kth approximation to the attractor in the quasiperiodically-forced system. For this rational approximation of level k, it is sufficient to change the initial phase θ_0 in the interval $[0, 1/F_k)$ in order to get all possible attracting sets because the set of all θ values fills the whole interval $[0, 1)$.

We consider the rational approximation of level $k = 6$ for $A_2 = 0.3$ μA/cm^2. As shown in Fig. 4(a) for $I_{dc} = 1.9$ μA/cm^2, the rational approximation to a stable smooth torus (represented by the black curve), corresponding to a silent state, consists of stable orbits with period F_6 $(= 8)$. On the other hand, the rational approximation to an unstable smooth torus (denoted by the gray curve) consists of unstable F_6-periodic orbits and lies very close to the stable torus [see a magnified view near $F_6\theta = 0.5$ in Fig. 4(b)]. As I_{dc} passes a threshold value $I^{(6)}_{dc}$($\simeq$1.9375 μA/cm^2), a phase-dependent saddle-node bifurcation occurs through collision of the stable and the unstable tori at specific θ-values (not at all θ values). As a result, "gaps," where no orbits with period F_6 exist, are formed. A magnified gap is shown in Fig. 4(c) for $I_{dc} = 2.6$ μA/cm^2. Note that this gap is filled with intermittent chaotic attractors, together with orbits with regular attractors with periods higher than F_6 embedded in very small windows. As shown in Fig. 4(d), the rational approximation to the whole attractor consists of the union of the periodic component and the intermittent chaotic component, where the latter occupies the F_6 gaps in θ. Figure 4(e) shows the Lyapunov-exponent diagram (*i.e.*, plot of $\sigma_1(\theta)$ vs. $F_6\theta$) for $I_{\rm dc} = 2.6$ μA/cm^2. The

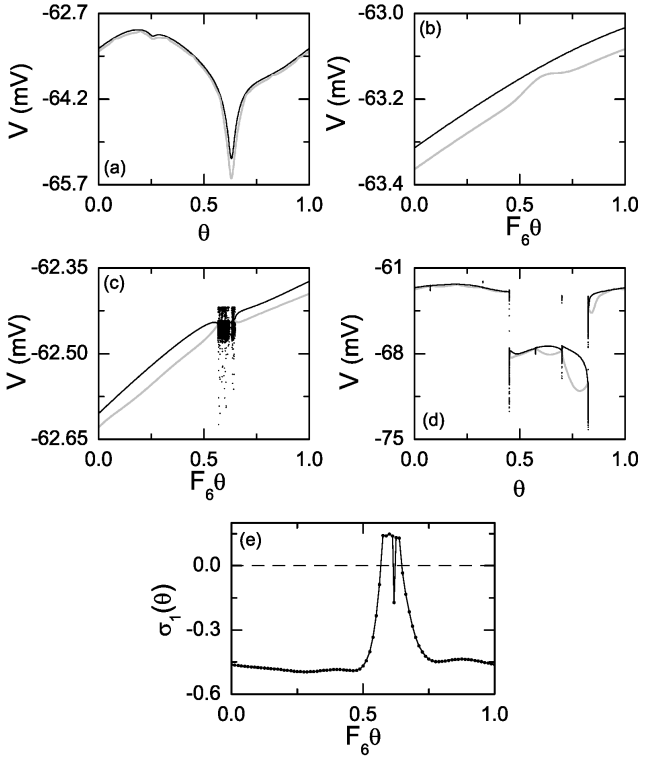

Fig. 4. Investigation of the transition from a smooth torus (corresponding to a silent state) to an SN attractor (corresponding to an SN spiking state) in the rational approximation of level $k = 6$ for $A_1 = 1.0$ μA/cm^2, $A_2 = 0.3$ μA/cm^2, and $f_1 = 60$ Hz. (a) Smooth stable and unstable tori for $I_{dc} = 1.9$ μA/cm^2. The unstable torus (shown in gray) lies very close to the stable torus (shown in black). A magnified view near $F_6\theta = 0.5$ is given in (b). (c) and (d) The 6th rational approximation to the intermittent SN attractor for $I_{dc} = 2.6$ μA/cm^2. A magnified gap near $F_6\theta = 0.5$ is given in (c). (e) Lyapunov-exponent diagram for $I_{\rm dc} = 2.6$ μA/cm^2 in the Poincaré map.

angle-averaged Lyapunov exponent $\langle\sigma_1\rangle$ [$\langle\cdots\rangle$ denotes the average over the whole θ] is given by the sum of the "weighted" Lyapunov exponents of the periodic and the chaotic components, Λ_p and Λ_c, (*i.e.*, $\langle\sigma_1\rangle = \Lambda_p + \Lambda_c$), where $\Lambda_{p(c)} = M_{p(c)}\langle\sigma_1\rangle_{p(c)}$, and $M_{p(c)}$ and $\langle\sigma_1\rangle_{p(c)}$ are the Lebesgue measure in θ and the average Lyapunov exponent of the periodic (chaotic) component, respectively. Since the periodic component is dominant, the average Lyapunov exponent ($\langle\sigma_1\rangle \simeq -0.392$) is negative. Hence, the rational approximation to the spiking attractor in Fig. 4(d) is nonchaotic. We note that Fig. 4(d) resembles Fig. 3(b), although the level $k = 6$ is low. Increasing the level to $k = 10$, we confirm that the rational approximations to the whole attractor have F_k gaps (filled with intermittent chaotic attractors), which appear via phase-dependent saddle-node bifurcations and that their average Lyapunov exponents are negative. In this way, an SN spiking attractor appears in the case of quasiperiodic forcing, as shown in Fig. 3(b).

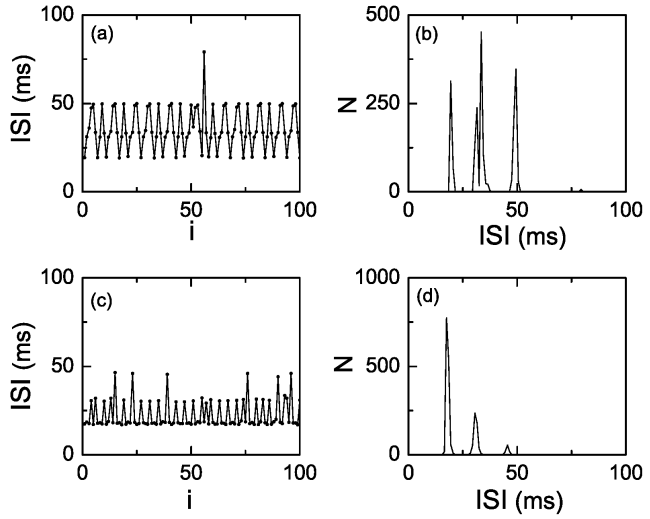

Fig. 5. Characterization of the SN ($I_{dc} = 2.85\,\mu$A/cm^2) and the chaotic ($I_{dc} = 3.9\,\mu$A/cm^2) spiking states for $A_1 = 1.0\ \mu$A/cm^2, $A_2 = 0.3\ \mu$A/cm^2, and $f_1 = 60$ Hz. Sequences of interspike intervals for (a) SN and (c) chaotic spikings; i represents the spiking index. Histograms of the interspike intervals for (b) SN and (d) chaotic spikings. For histograms of ISI, 200 equally-spaced bins are chosen in the range of ISI $\in (0, 100)$. We get the number of spikes (N) in each bin from a total number of 2000 spikes.

Finally, we characterize both the SN and the chaotic spiking states for $A_2 = 0.3\ \mu$A/cm^2 in terms of the interspike interval. Figures 5(a) and 5(c) show sequences of the interspike intervals for the SN and chaotic spiking states when $I_{dc} = 2.85$ and $3.9\ \mu$A/cm^2, respectively. Both sequences are aperiodic complex ones. Histograms for the interspike intervals for the SN and the chaotic spiking states are also given in Figs. 5(b) and 5(d), respectively. They are multimodal ones. As I_{dc} is increased, the heights of the peaks for short interspike intervals increase, while those for longer ones decrease. Hence, the average interspike interval decreases (*i.e.*, the mean spiking rate increases) as I_{dc} is increased. Thus, both the SN and the chaotic spiking states exhibit aperiodic complex spikings, although their dynamics are different (one is chaotic and the other one is nonchaotic). We note that such aperiodic complexity results from the strange geometry of the SN and the chaotic spiking states.

III. SUMMARY

We have investigated the dynamical transition from a silent state to a spiking state by varying the dc stimulus I_{dc} in the quasiperiodically forced HH neuron. For this quasiperiodically-forced case, a transition from a silent state to an SN spiking state (with negative Lyapunov exponent and positive phase-sensitivity exponent) has been found to occur when I_{dc} passes a threshold value. With a further increase in I_{dc}, such an SN spiking state transforms to a chaotic spiking state (with a positive Lyapunov exponent). Thus, a new type of SN spiking state appears between the silent state and the chaotic spiking state as an intermediate one. Using a rational approximation to the quasiperiodic forcing, we have studied the mechanism for the appearance of SN spiking states. Thus, a smooth torus, corresponding to a silent state, is found to transform to an SN spiking attractor through a phase-dependent saddle-node bifurcation. Both the SN and the chaotic spiking states have been characterized in terms of the interspike interval. As a result of their strange geometry, both spiking states are found to be aperiodic complex ones, although their dynamics are qualitatively different. These kinds of complex spikings might be one of the origins of complex physiological bodily rhythms.

ACKNOWLEDGMENTS

This research was supported by the Basic Science Research Program through the National Research Foundation of Korea funded by the Ministry of Education, Science and Technology (2009-0070865).

REFERENCES

[1] M. R. Guevara, L. Glass and A. Shrier, Science **214**, 1350 (1981); L. Glass, M. R. Guevara, A. Shrier and R. Perez, Physica D **7**, 89 (1983).
[2] K. Aihara, T. Numajiri, G. Matsumoto and M. Kotani, Phys. Lett. A **116**, 313 (1986); N. Takahashi, Y. Hanyu, T. Musha, R. Kubo and G. Matsumoto, Physica D **43**, 318 (1990); D. T. Kaplan, J. R. Clay, T. Manning, L. Glass, M. R. Guevara and A. Shrier, Phys. Rev. Lett. **76**, 4074 (1996).
[3] K. Aihara, Scholarpedia **3**, 1786 (2008) and see also references therein.
[4] R. Stoop, K. Schindler and L. A. Bunimovich, Neurosci. Res. **36**, 81 (2000); Nonlinearity **13**, 1515 (2000).
[5] L. Glass and M. C. Mackey, *From Clocks to Chaos* (Princeton University Press, Princeton, 1988).
[6] L. Glass, Nature **410**, 277 (2001).
[7] M. Ding and J. A. S. Kelso, Int. J. Bifurcation Chaos Appl. Sci. Eng. **4**, 553 (1994).
[8] W. Lim, S.-Y. Kim and Y. Kim, Prog. Theor. Phys. **121**, 671 (2009); W. Lim and S.-Y. Kim, J. Phys. A **42**, 265103 (2009).
[9] C. Grebogi, E. Ott, S. Pelikan and J. A. Yorke, Physica D **13**, 261 (1984).
[10] U. Feudel, S. Kuznetsov and A. Pikovsky, *Strange Nonchaotic Attractors* (World Scientific, Singapore, 2006) and see also references therein.
[11] A. S. Pikovsky and U. Feudel, Chaos **5**, 253 (1995).
[12] S.-Y. Kim, W. Lim and E. Ott, Phys. Rev. E **67**, 056203 (2003); S.-Y. Kim and W. Lim, J. Phys. A **37**, 6477

(2004); Phys. Lett. A **334**, 160 (2005); W. Lim and S.-Y. Kim, *ibid.* **335**, 383 (2005); *ibid.* **355**, 331 (2006); J.-W. Kim, S.-Y. Kim, B. Hunt and E. Ott, Phys. Rev. E **67**, 036211 (2003).

[13] A. L. Hodgkin and A. F. Huxley, J. Physiol. (London) **117**, 500 (1952).

[14] K. Aihara, G. Matsumoto and Y. Ikegaya, J. Theor. Biol. **109**, 249 (1984).

[15] D. Hansel, G. Mato and C. Meunier, Europhys. Lett. **23**, 367 (1993).

[16] A. J. Lichtenberg and M. A. Lieberman, *Regular and Stochastic Motion* (Springer-Verlag, New York, 1983), p. 283; A. Wolf, J. B. Swift, H. L. Swinney and J. A. Vastano, Physica D **16**, 285 (1985).